Hindawi
Geofluids
Volume 2022, Article ID 3464456, 13 pages
https://doi.org/10.1155/2022/3464456

Research Article

Exploration of the Relationships between the Spraying Condition and Wetting Behavior on Coal Surface of Dust Suppression Droplet: Improving the Utilization Rate

Fangwei Han,[1,2] **Jian Li**,[1] **Yingying Peng**,[1] **and Yue Zhao**[1]

[1]*College of Safety Science and Engineering, Liaoning Technical University, Huludao, Liaoning 125105, China*
[2]*Key Laboratory of Mine Thermodynamic Disasters and Control, Ministry of Education, Liaoning Technical University, Huludao, Liaoning 125105, China*

Correspondence should be addressed to Fangwei Han; hanfangweixinxiang@163.com

Received 16 October 2022; Revised 3 December 2022; Accepted 9 December 2022; Published 21 December 2022

Academic Editor: Hetang Wang

Dust suppression through water-based media is an important technical means, which is of great significance to industrial process safety and environmental protection. In order to improve the utilization rate of droplets, the dynamic spreading process of droplets impacting the coal surface was studied by the coupled level-set and volume-of-fluid methods (CLSVOF) method. The spread area was calculated by the binary method to characterize the wetting effect. Dimensionless spread area per unit volume (DSAPUV) was proposed to represent the utilization of droplets. The results show that the droplet spreading fracture process can be divided into three stages: initial deformation period, spreading fracture period, and stable period. When the particle size was not being changed, the area of dimensionless spread does not increase consistently with velocities, but there exists an optimal critical velocity of impingement, which is 17 m/s for the maximum dimensionless spread area reached by droplets with a diameter of 30 μm and 19 m/s for the maximum dimensionless spread area reached by droplets with a diameter of 50 μm. Droplet size is directly proportional to the dimensionless spread area. The maximum dimensionless spread areas of the droplets were all reached during spreading, and the time required increased gradually with increasing particle sizes. It was found that the effect of droplet size on the utilization of droplets was obvious when their size ranged from 10 μm to 50 μm, and their velocity ranged from 15 m/s to 20 m/s.

1. Introduction

Coal dust threatens the safety production and environmental protection of mines. It can burn and explode, and cause extremely serious accidents and losses [1–5]. On the other hand, coal dust negatively impacts the air quality in the mining area and causes severe health hazards. The adverse effects of exposure to coal dust during operation on miners' health have been recognized as a paramount issue. During the last 2 decades, lung diseases among coal miners have resurged in several countries [6–11]. In addition, coal dust particles will also strengthen the wear of equipment and reduce its reliability and accuracy. Therefore, the suppression and prevention of coal dust are very important.

Whether in open-pit coal mines or underground coal mines, spraying water-based materials is an important means of dust suppression and control [12–15]. This technology is of great significance to safety production and environmental protection. After the droplet impacts the coal surface, it can spread, retract, and break up, which has obvious dynamic characteristics. However, the existing studies of coal wetting mainly observe the static wetting characteristics or slow wetting characteristics of droplets on the coal surface. Based on this, the wettability of droplets on the coal surface is evaluated. The commonly used evaluation methods mainly include the sessile drop method, the sedimentation method, the capillary rise method, the infiltration method, and so on.

The sessile drop method is the most widely used method, which forms three-phase contact by slowly dropping a droplet on the tablet [16–18]. A contact angle less than 90° means high wettability, while a contact angle greater than 90° corresponds to low wettability. Cheng et al., Zhou et al., and Li et al. analyzed and optimized the coal wetting agent with the contact angle as the evaluation index and achieved a good dust control effect [19–21]. Chen et al. further optimized and improved the sessile drop method and proposed the volume-length (VL) method to measure the contact angle. The VL method ignores the influence of infiltration or evaporation on the measurement and can measure the initial contact angle and the maximum contact angle [22]. Cheng et al. found that the contact angle of coal dust increases with the increase of its infrared transmittance. When the transmittance exceeds 30%, the contact angle is large and stable [23]. Gui et al. studied the influencing factors of coal dust wettability through experiments and found that the contact angle is not the decisive factor for evaluating surfactants [24]. The sedimentation method indirectly characterizes the wettability by measuring the time required for all quantitative dust to settle into the test solution or by measuring the mass fraction of dust particles immersed in water from the thin dust layer sprinkled on the solution surface within a certain time. The sedimentation experiment is affected by the particle size distribution and the uniformity of powder spraying. Therefore, it is necessary to repeat three to five times to improve accuracy [25, 26]. The capillary rise test is a method to evaluate the wettability by using the capillary rise of liquid in the test tube containing dust particles [27–29]. In this method, the evaluation index is the time required for solution penetration per unit height or the penetration height per unit time. The permeation rate of the solution to the powder bed was measured by the permeation experiment [30].

It can be observed that the research on the wettability of water-based materials to coal is mainly static and slow wetting, while the research on dynamic wetting is less. There are obvious limitations in using these methods to evaluate the wettability of droplets in the process of impacting the coal surface. In engineering practice, the behavior of droplets impacting the coal surface widely exists in the dust control process. The dynamic behavior of droplets is extremely complex. There are obvious dynamic processes such as spreading, retraction, and rebounding. The time scale of droplets gradually spreading and penetration on the coal surface is much greater than the impact contact time between droplets and coal, that is, the time before the droplet rebounding, splashing, or breaking on the coal surface. Considering the relevant dynamic factors, this impacting method can better reflect the actual wetting characteristics and application effects.

In this paper, the numerical simulation method, coupled level-set and volume-of-fluid methods (CLSVOF) is used to study the wetting phenomenon of droplets after impacting the coal surface under different conditions, and its dynamic spreading behavior is analyzed. A new evaluating indicator "dimensionless spread area per unit volume (DSAPUV)" was proposed to represent the utilization of droplets. This study is helpful to understand the dynamic wetting process when droplets impact on the coal surface and optimizing the utilization rate of dust suppression droplets on the coal surface.

2. Simulation Method and Verification

2.1. Simulation Method. The morphology of the microdroplet is tracked by CLSVOF method, which was proposed by Sussman et al. [31, 32]. The method combines the good conservation of the volume-of-fluid (VOF) method with the advantages of the level-set (LS) method to deal with the local sharp corners of the interface. The coupling of both LS and VOF methods ensures mass conservation, the ability to capture the free surface, and to correctly compute the surface tension force.

In the VOF method, the phase interface is captured by calculating the volume fraction in each element [33–35]. Different fluid components share a set of momentum equations. The volume fraction of each fluid component is recorded in each calculation cell. The transient Navier-Stokes equations are solved using a finite-difference formulation on a fixed grid. According to the conservation of mass, the continuity equation is shown in

$$\frac{\partial a_{\mathrm{liq}}}{\partial t} + \vec{V} \cdot \nabla a_{\mathrm{liq}} = 0, \tag{1}$$

where t is the time, $\vec{V}$ is the velocity vector, and a_{liq} is the volume fraction of liquid phase. $a_{\mathrm{liq}} = 0$ means that the gas phase is in the grid, $a_{\mathrm{liq}} = 1$ means that the grid is full of liquid phase, and $0 < a_{\mathrm{liq}} < 1$ means that the interface is in the grid.

The momentum equation is shown in

$$\frac{\partial}{\partial t}\left(\rho\vec{V}\right) + \vec{V} \cdot \left(\rho\vec{V}\vec{V}\right) = -\nabla p + \nabla \cdot \left[\mu\left(\nabla\vec{V} + \nabla\vec{V}^{T}\right)\right] + \rho\vec{g} + \vec{F}, \tag{2}$$

where t is the time, $\vec{V}$ is the velocity vector, p is the pressure, ρ is the density, μ is the dynamic viscosity, $\vec{g}$ is the acceleration of gravity, and $\vec{F}$ is the volume force.

The interface position and time evolution equation are defined by LS method, as shown in

$$\frac{D\phi}{\mathrm{Dt}} = \frac{\delta\phi}{\delta t} + (v \bullet \nabla)\phi = 0, \tag{3}$$

where v is the velocity of the flow field.

Equation (3) is the convective transport equation of function ϕ, which is rewritten into the following form as shown in Equation (4) in order to transform to the discrete solution easily:

$$\frac{\delta\phi}{\delta t} + v(\nabla \bullet \phi) = 0, \tag{4}$$

where ϕ is defined as the distance function to the interface between the liquid and gas, and Ω is the material region in the level-set method. So, the interface is a zero-level set, and $\phi(x, t)$ is expressed as $\Gamma = \{x \in \Omega | \phi(x, t) = 0\}$ in a two-phase system. There are three conditions as shown in

$$\phi(x, t) = \begin{cases} +|d|, \\ 0, \\ -|d|, \end{cases} \tag{5}$$

where d is the distance from x to the interface. $\phi = 0$ means x at the interface of the two phases, $\phi > 0$ means x in the liquid phase, and $\phi < 0$ means x in the gas phase. All the possible distance from the specified point to the interface has been minimized in order to initialize the ϕ function. The normal vector and curvature of the interface required to calculate surface tension can be estimated in Equation (6) and Equation (7), respectively.

$$n = \left. \frac{\nabla \phi}{|\nabla \phi|} \right|_{\phi=0}, \tag{6}$$

$$k = \nabla \cdot = \left. \frac{\nabla \phi}{|\nabla \phi|} \right|_{\phi=0}. \tag{7}$$

The numerical instability resulting from the ratio of the large density and large viscosity near the interface has been avoided by the Heaviside function which is introduced to smooth the density and viscosity at the interface. The Heaviside function is shown in

$$H(\phi) = \begin{cases} 0, & \phi < -w, \\ \frac{1}{2}\left[1 + \frac{\phi}{w} - \frac{1}{\pi} \sin\left(\frac{\pi\phi}{w}\right)\right], & |\phi| \le w, \\ 1, & \phi > w, \end{cases} \tag{8}$$

where $w = 1.5h$ (h is the grid size). The density and viscosity are shown in Equation (9) and Equation (10), respectively.

$$\rho(\phi) = \rho_g + \left(\rho_1 - \rho_g\right) H(\phi), \tag{9}$$

$$\mu(\phi) = \mu_g + \left(\mu_1 - \mu_g\right) H(\phi). \tag{10}$$

The idea of piecewise linear geometric reconstruction is used to reconstruct the interface, and line segments are used to replace the interface in a single grid. The difference is that the normal vector of the interface is calculated by the level set function. The VOF method is used to solve the volume fraction in the grid and reconstruct the interface in the grid.

Pressure–velocity coupling is achieved by the PISO algorithm. Discretization of the momentum flux term is achieved by a second-order upwind scheme, while for the time discretization, a first-order implicit approach is followed for the momentum equation. The quick algorithm is used to solve the level set equation. The volume fraction equation is solved in an explicit manner at the beginning of each time step, using the velocity values derived during the previous time step as input.

Table 1: Numerical simulation parameter settings.

Serial number	Parameters	Value
1	Gas pressure	101325 pa
2	Droplet density	998.2 kg·m^{-3}
3	Droplet viscosity	1.003×10^{-3} pa·s
4	Droplet surface tension	0.072 N·m^{-1}
5	Air density	1.225 kg·m^{-3}
6	Air viscosity	1.7894×10^{-5} pa·s
7	Coal surface contact angle	60°
8	Coal surface roughness height	24.3 nm
9	Coal surface roughness constant	0.5

2.2. Parameter Setting. When using water sprays, one of the primary considerations is the droplet size. For dust suppression, the size of water droplets should be within an appropriate range. Previous studies have shown that in dust removal practice, droplets with particle sizes in the range of 10 μm~150 μm have been proven to be the most effective [36]. In view of this, and considering the dust suppression efficiency and spray cost, 10 μm, 30 μm, and 50 μm were selected for the droplet size in this study.

The simulated ambient pressure is the ideal standard atmospheric pressure, and the influence of external disturbance airflow on the impact process is not considered. Relevant parameter settings are shown in Table 1.

In this paper, the dimensionless spread area (DSA), S^* is used to characterize the spreading and wetting of droplets on the coal surface. S^* is calculated as shown in

$$S^* = \frac{S}{S_0}, \tag{11}$$

where S is the spread area of droplets on the coal surface; S_0 is the initial surface area of the droplet.

When droplets with different particle sizes hit the coal surface, the comparison of the spread area cannot explain the utilization rate of droplets. However, the dimensionless spread area per unit volume (DSAPUV) characterizes the wetting effect and reflects the utilization rate of droplets, which is helpful for more accurate cost control. Therefore, the dimensionless spread area per unit volume (DSAPUV) is proposed and its calculation is shown in

$$A = \frac{S^*}{V}, \tag{12}$$

where A is DSAPUV and V is the droplet volume.

2.3. Experimental Verifications. To verify the rationality of the model and the reliability of the simulation method, a

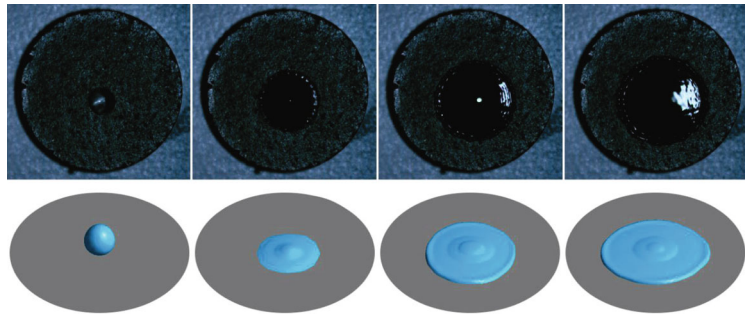

Figure 1: Experimental and simulation results of the droplet impact on coal surface.

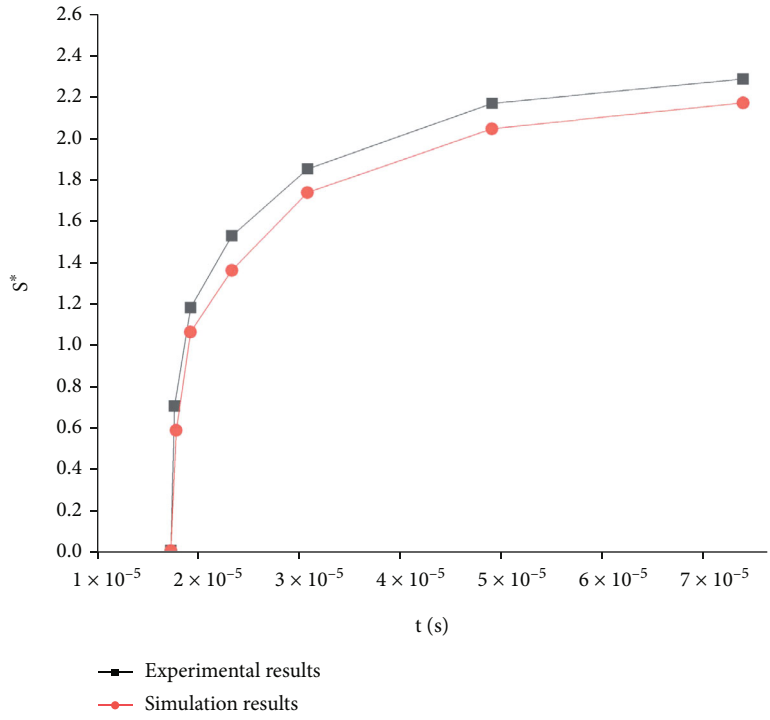

Figure 2: Variation trend of dimensionless spread area with time in the experiment and simulation.

high-speed camera (VEO340s) is used to experimentally study the dynamic spreading process of droplets impacting the coal surface. During the experiment, the droplets were driven out of a needle by a peristaltic pump. When the needle flow is 1 ml/min, the drop diameter is 2 mm. The droplets vertically impact the coal surface in the form of free fall. By modifying the distance between the needle and the coal surface, the impact velocity can be adjusted. The velocity of droplets impacting the coal surface is 1 m/s. Figure 1 shows the deformation process of droplets after impacting the coal surface obtained by the experiment and numerical simulation. It can be found that the two are basically the same.

The change of the dimensionless spread area with time obtained by the experiment and simulation is presented in Figure 2. The simulation results are in good agreement with the experiments. The small error is caused by the simulation method and model meshing, which do not affect the analysis of the deformation process of droplets impacting the coal surface. Therefore, this simulation method can be used in this research work.

3. Results and Discussion

3.1. Influence of Impact Velocity on Spreading Effect. Figure 3(a) shows the change of dimensionless spread area (DSA) with dimensionless time during the impact of a droplet ($D_0 = 10\,\mu$m) on the coal surface at different speeds. It can be found that when $V_0 = 15$ m/s, the maximum DSA is 4.33. With the increase in speed, the maximum DSA gradually increases. When $V_0 = 20$ m/s, the maximum DSA of droplets reaches 5.78. This is because the larger the initial velocity is, the more kinetic energy the droplet has, and the more prone it is to spread [37, 38]. However, when the speed increases gradually, the dimensionless time required to reach the maximum DSA first increases and then decreases. This is

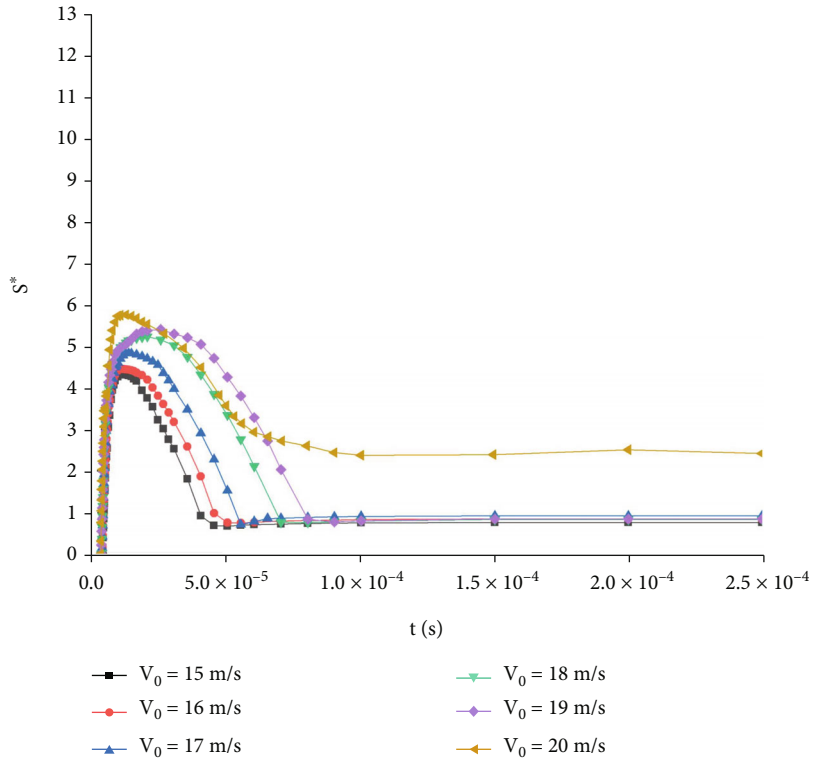

(a) $D_0 = 10\,\mu$m

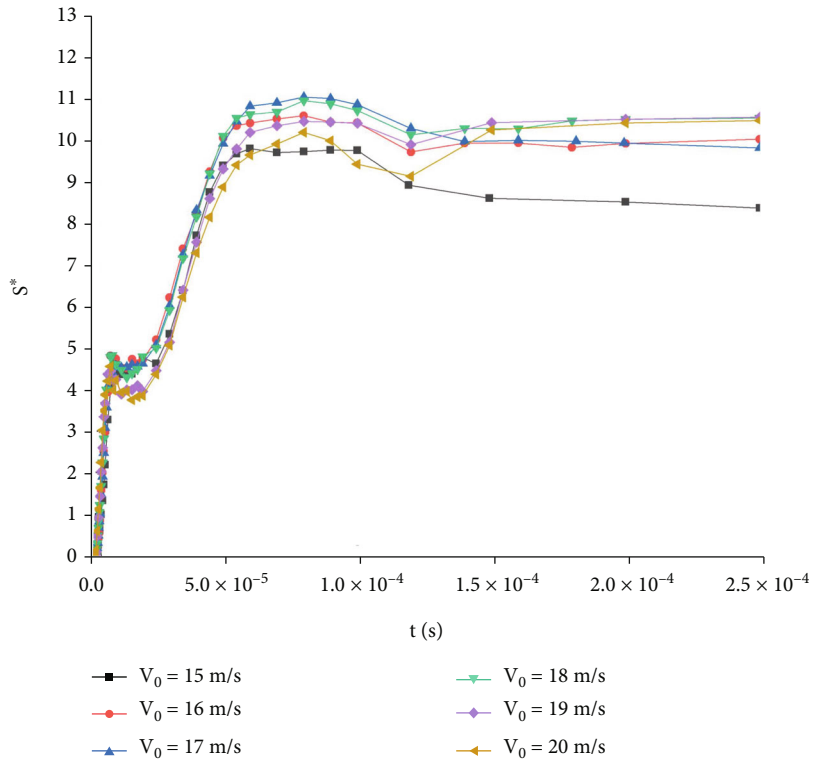

(b) $D_0 = 30\,\mu$m

Figure 3: Continued.

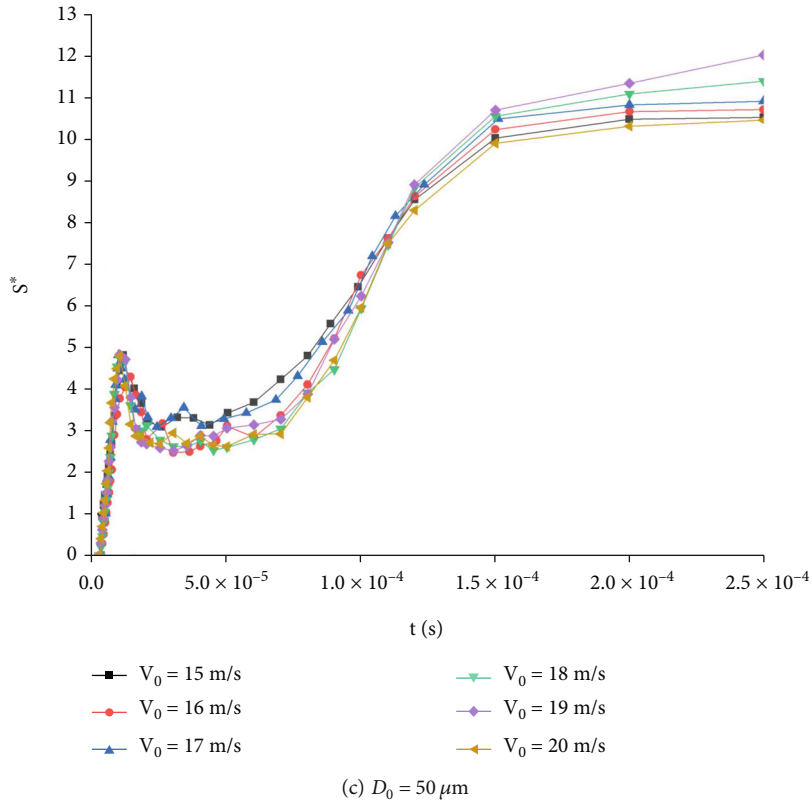

(c) $D_0 = 50\,\mu$m

Figure 3: Dimensionless spread area of droplets at different velocities over time.

because the higher the velocity is, the more kinetic energy the droplet has, and the longer the dimensionless time required for the kinetic energy to be fully dissipated in the spreading process. However, when the velocity further increases, the droplets split, and each subdroplet spreads at the same time, so the kinetic energy dissipation is accelerated and the dimensionless time required to reach the maximum DSA is reduced.

As can be seen from Figure 3(b), when the droplet diameter is 30 μm and V_0 is between 15 m/s and 17 m/s, the maximum DSA increases from 9.86 to 11.06; when V_0 is between 17 m/s and 20 m/s, the maximum DSA is reduced from 11.06 to 10.50. So, when $V_0 = 17$ m/s, the maximum DSA is the largest. The DSA first increases with the increase in speed. After it reaches the critical maximum, it decreases with the increase in velocity. By analyzing the simulation data, it can also be found that when V_0 is between 15 m/s and 20 m/s, the maximum DSA is reached in the spreading process. Because the kinetic energy in the early stage is mainly consumed in the spreading process, after reaching the maximum spread area, the retraction oscillation continues in the subsequent spreading period [39]. The remaining kinetic energy is continuously dissipated, so it is impossible to reach a larger spread area.

As can be seen from Figure 3(c), when the droplet diameter is 50 μm and V_0 is between 15 m/s and 19 m/s, the maximum DSA increases from 10.59 to 12.09; V_0 is between 19 m/s and 20 m/s, the maximum DSA is reduced to 10.52. So, when $V_0 = 19$ m/s, the maximum DSA is the largest. The DSA first increases with the increase in velocity. After it reaches a critical maximum, it decreases with the increase in velocity. The spreading and oscillation process of 50 μm droplets is more significant than that of 30 μm droplets. This is because the droplet with a diameter of 50 μm has a larger mass, more initial kinetic energy, and high dispersion fracture occurs earlier. Each separated subdroplet continues to oscillate and spread under the synergistic action of residual kinetic energy, surface energy, and viscous dissipation [40]. When the kinetic energy of subdroplets is exhausted, subdroplets begin to retract under the effect of surface tension, and the more subdroplets, the smaller DSA. The maximum DSA is significantly higher than that of 30 μm droplets, and the spreading dimensionless time is relatively large.

To sum up, when the droplet size is 10 μm, the maximum DSA is reached when the impact speed is 20 m/s; when the droplet size is the 30 μm, the maximum DSA is reached when the impact speed is 17 m/s; when the droplet size is 50 μm, the maximum DSA is reached when the impact speed is 19 m/s. It can be seen that in the practice of dust suppression, the droplet size and its impact speed should be optimized and matched to achieve the best wetting effect.

3.2. Influence of Droplet Size on Spreading Effect. In order to further study the spreading behavior of droplets on the coal surface, droplets with diameters of 10 μm, 30 μm, and 50 μm were simulated and analyzed at the same speed. Figure 4 shows the evolution of the DSA over time when droplets with different sizes impact the coal surface at the impact

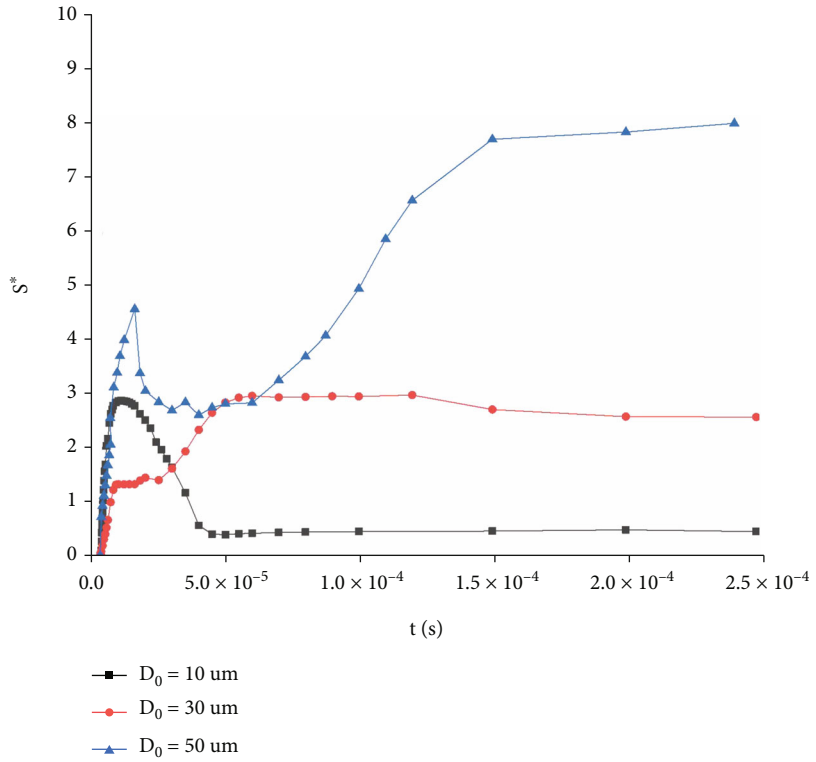

(a) $V_0 = 15$ m/s

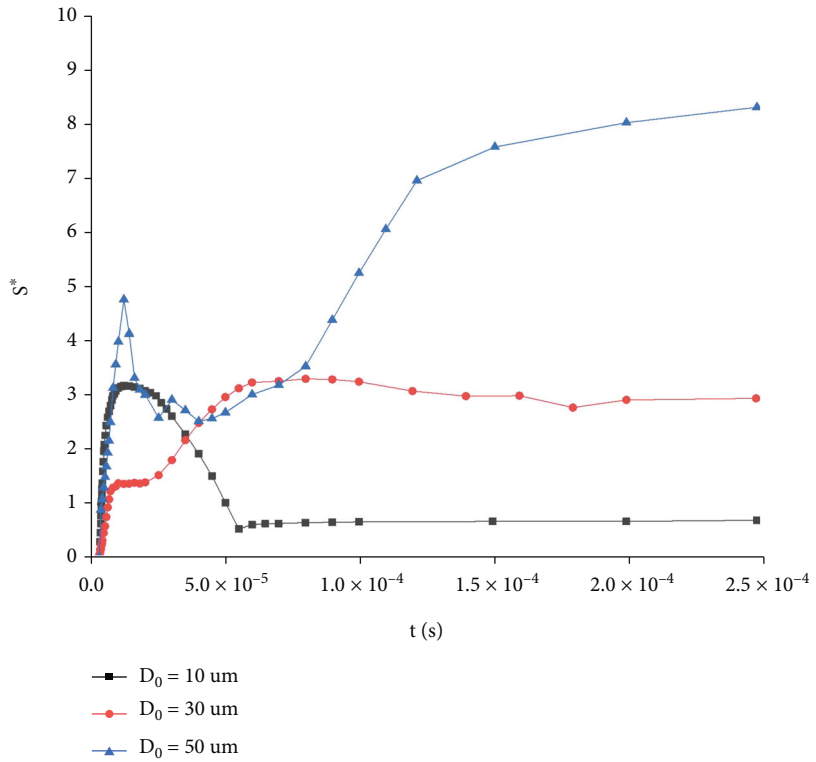

(b) $V_0 = 17$ m/s

Figure 4: Continued.

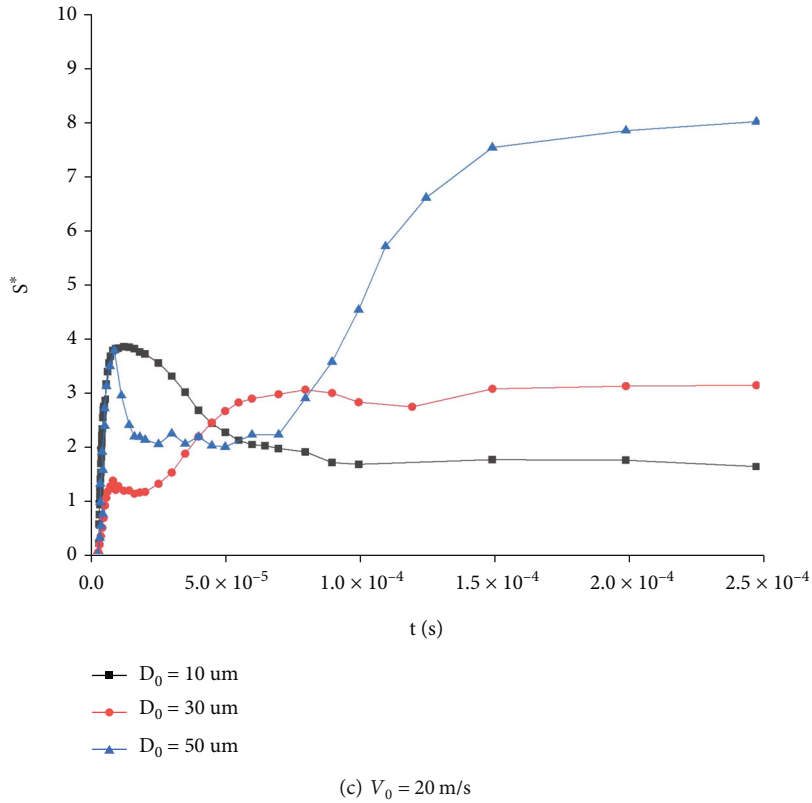

(c) $V_0 = 20$ m/s

Figure 4: Dimensionless spread area of droplets with different particle sizes over time.

velocities of 15 m/s, 17 m/s, and 20 m/s, respectively. It can be found that at the same velocity, the time required to reach the maximum DSA and the spread area increases as the droplet diameter increases. This is because at the same speed, the larger the droplet size is, the greater the total kinetic energy is, and the more difficult it is for the droplet surface tension and viscous force to restrain the inertia-dominated spreading behavior after colliding with the coal surface.

As shown in Figure 5, droplets with a diameter of 10 μm first diffuse and spread into a disk shape after impact. Due to the larger velocity at the outer edge of the droplet and the smaller velocity at the center, the droplet breaks from the center to form a liquid ring. In this process, part of the kinetic energy is converted into deformation potential energy and friction dissipation. When the spreading speed of the outer edge of the liquid ring decreases to 0, the liquid ring begins to retract and finally converge into droplets under the action of viscous force and surface tension. With the gradual increase of droplet impact velocity, the fracture trend becomes stronger. When the impact velocity is 20 m/s, the droplet breaks into multiple liquid rings and eventually forms multiple subdroplets.

When the droplet diameter is 30 μm, the spreading and fracture phenomena become more and more obvious, as shown in Figure 6. After the droplet impacts the coal surface, it quickly breaks into multiple liquid rings. Then, liquid rings split into multiple subdroplets. This is due to the droplet volume being larger, surface tension cannot pull the droplet back greatly after hitting the coal surface. The subdroplets retract under the action of surface tension. Finally, the subdroplets are arranged in a ring shape. The larger the initial velocity of droplets, the more liquid rings are formed by fragmentation, and the more subdroplets are in a steady state. Shape changes of droplets with a diameter of 50 μm impacting the coal surface are similar to that of droplets with a diameter of 30 μm, due to the larger mass, more overall kinetic energy, and more subdroplets produced by crushing.

3.3. Droplet Utilization Analyses. Figure 7 shows the change of dimensionless spread area per unit volume (DSAPUV) with time under different conditions. It can be seen that the DSAPUV of droplets with a diameter of 50 μm is the largest. In addition, at the same speed, when the spreading tends to be stable, the increase in particle size can lead to an obvious increase in droplet utilization. However, the improvement of droplet utilization is relatively limited by the small increase in speed. This is because the kinetic energy of the droplet is directly proportional to the third power of the droplet size and the second power of the velocity. The larger the droplet size is, the more obvious the increase of initial kinetic energy is. Finally, the droplet can achieve a better wetting effect and higher droplet utilization rate. When the particle size is the same and the velocity increases only slightly, the increase of overall kinetic energy is small, so the improvement of utilization is not obvious.

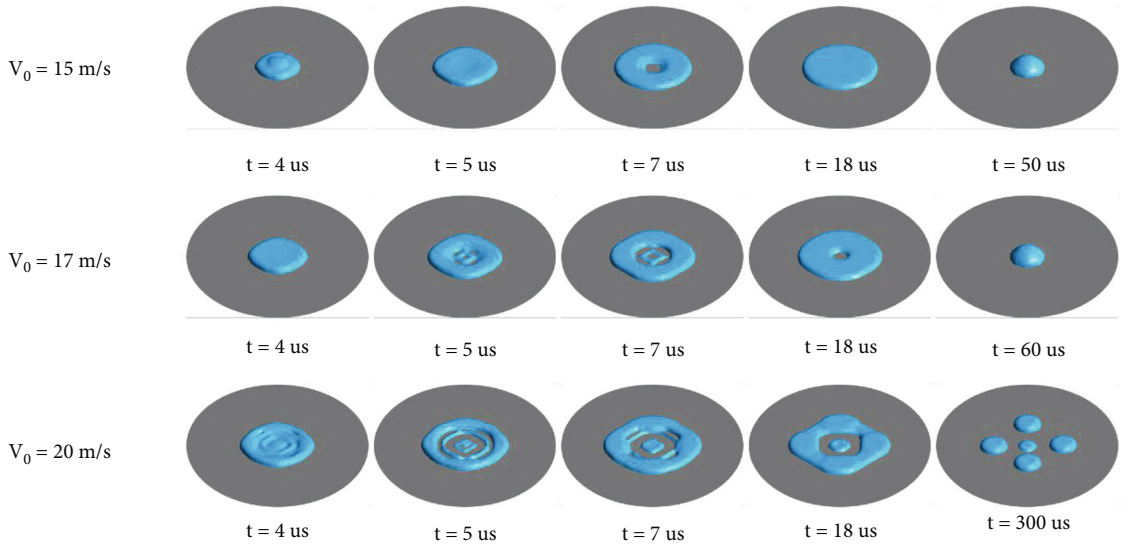

Figure 5: Spreading process of the droplet with a diameter of 10 μm.

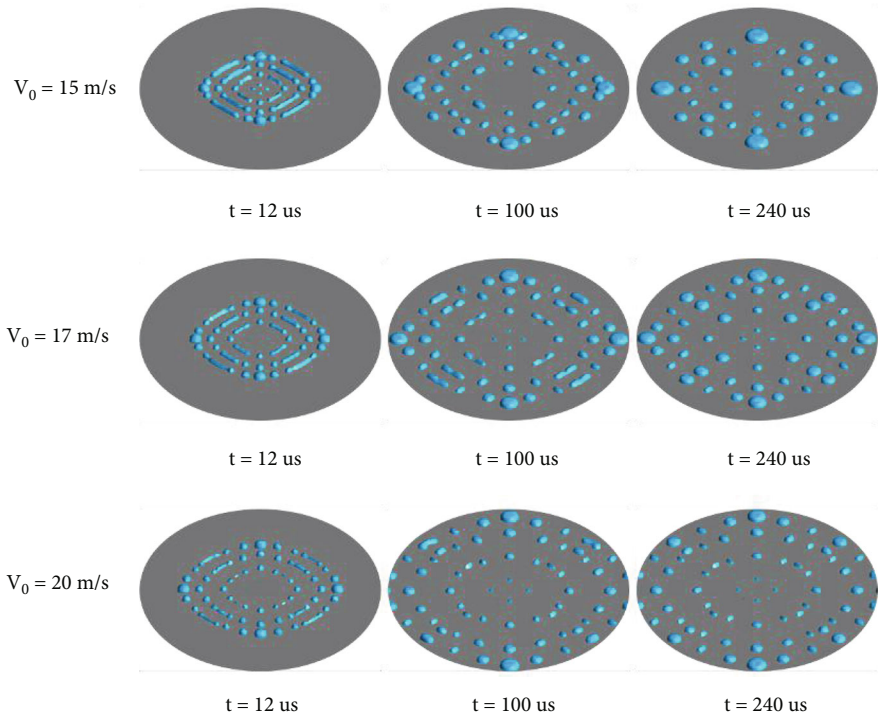

Figure 6: Spreading process of droplets with diameter of 30 μm.

According to the changing trend of the droplet utilization during impact, the spreading process can be divided into three periods: initial deformation period, oscillatory diffusion period, and stable period. During the initial deformation period, the droplets spread and deform rapidly from spherical to disk. At the same time, the DSAPUV also increased rapidly, and the droplet utilization rate increased significantly. In the period of oscillatory diffusion, the edge velocity of the liquid ring decreases gradually due to friction dissipation, and the liquid ring expands horizontally with internal contraction. This will lead to a decrease in DSAPUV and a decrease in droplet utilization. When the liquid ring retracts to a certain extent, the difference between the surface tension and the internal and external velocity of the liquid ring is not enough to make the liquid ring continue to retract. In the middle and late stages of oscillatory diffusion, the liquid ring breaks into subdroplets. Inertia force and residual kinetic energy make subdroplets spread

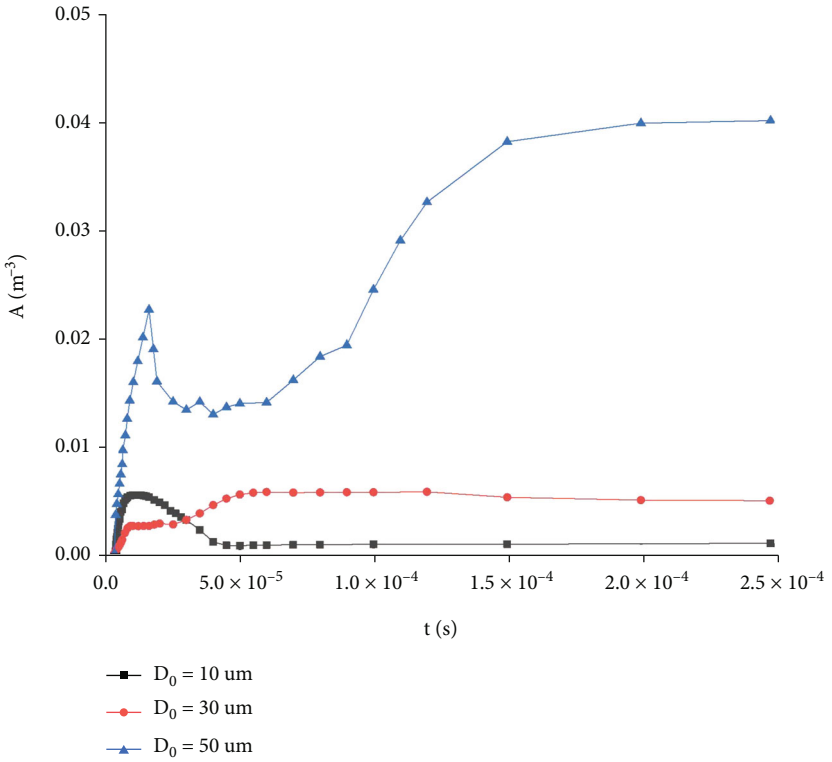

(a) $V_0 = 15$ m/s

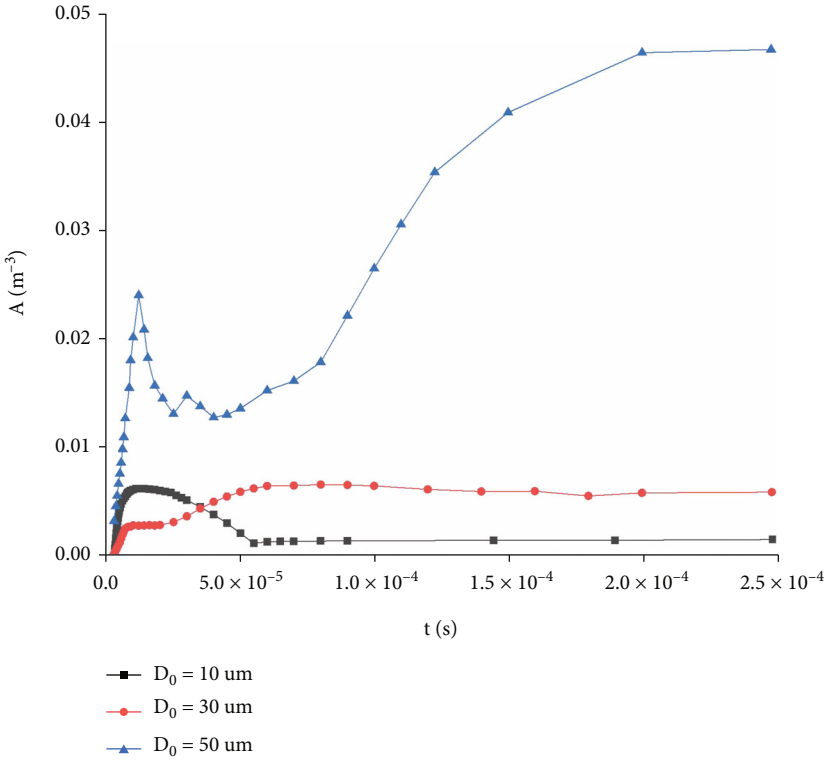

(b) $V_0 = 17$ m/s

Figure 7: Continued.

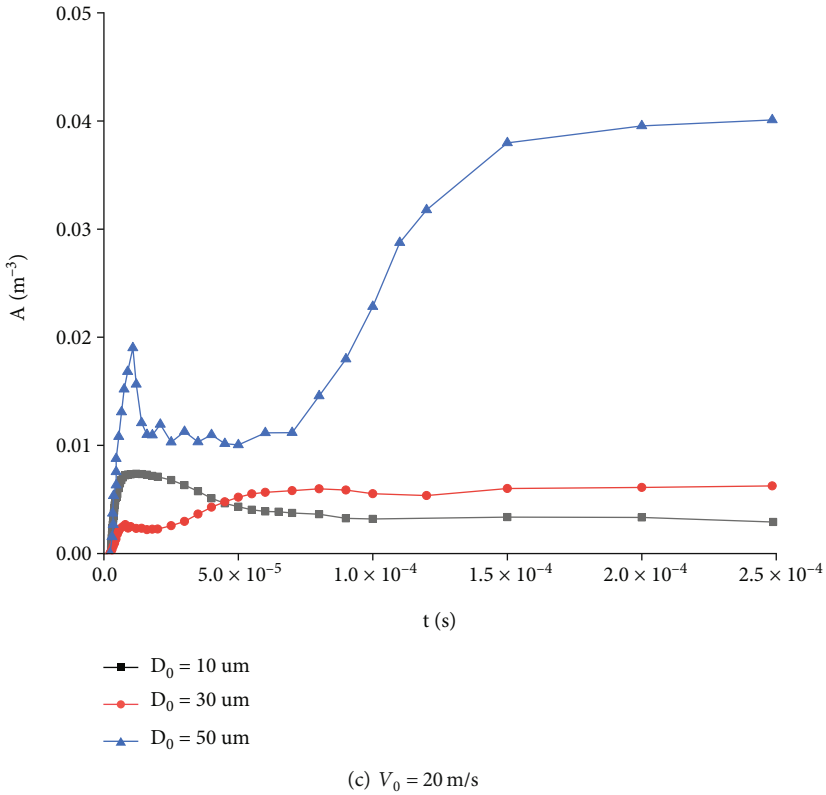

(c) V_0 = 20 m/s

Figure 7: Variation of dimensionless spread area of different droplets with time.

again. Currently, the DSAPUV increases significantly and the droplet utilization rate has increased. When entering the stable period, the internal kinetic energy of the droplet is almost completely dissipated, and the spreading range tends to be stable. Currently, the fluctuation of DSAPUV is small, and the droplet utilization rate tends to be stable.

4. Conclusions

In this paper, the wetting behavior of droplets with different diameters impacting the coal surface at speeds of 15 m/s ~20 m/s is studied. The following conclusions are drawn:

(1) The greater the droplet velocity, the more likely it is to fracture after spreading. Moreover, the number of liquid rings and subdroplets formed by the droplet fracture is also more. When the particle size and velocity are small, the liquid ring fracture will not occur in the spreading process and will eventually retract and converge into a droplet

(2) The larger the droplet size is, the longer it takes to reach the maximum dimensionless spread area after impact, and the larger the spread area is. DSAPUV can be used to compare droplet utilization under different particle sizes. When the droplet velocity is in the range of 15 m/s ~20 m/s and the particle size is in the range of 10 μm~50 μm, the particle size has a more significant effect on the droplet utilization than the velocity

(3) The spreading process can be divided into three periods: the initial deformation period, oscillatory diffusion period, and stable period. During the initial deformation period, the droplet utilization rate increased significantly. In the period of oscillating diffusion, the droplet utilization decreases first and then increases again. In the stable period, the droplet utilization rate tends to be stable in the equilibrium state

Data Availability

All data has been embedded in the manuscript.

Conflicts of Interest

The authors declare that they have no known competing financial interests or personal relationships that could have appeared to influence the work reported in this paper.

Authors' Contributions

Fangwei Han was tasked for the conceptualization, resources, methodology, writing the original draft, project administration, funding acquisition, and supervision. Jian Li contributed in the conceptualization, writing the original draft, investigation, and visualization. Yingying Peng worked in writing the original draft, conceptualization, data curation,

and methodology. Yue Zhao was responsible in writing the review and editing, data curation, formal analysis, and methodology.

Acknowledgments

This work was supported by the Natural Science Foundation of Liaoning Province (Grant number 2022-MS-396), the National Natural Science Foundation of China (Grant number 51604143), and the Research Grant of Key Laboratory of Mine Thermodynamic Disasters and Control, Ministry of Education, Liaoning Technical University (Grant number JSK202104). The authors deeply appreciate the support from the staff of Key Laboratory of Mine Thermodynamic Disasters and Control.

References

[1] L. Zhang, H. Y. Wang, C. Chen, P. P. Wang, and L. W. Xu, "Experimental study to assess the explosion hazard of CH_4/coal dust mixtures induced by high-temperature source surface," *Process Safety and Environment Protection*, vol. 154, pp. 60–71, 2021.

[2] H. T. Li, J. Deng, X. K. Chen et al., "Qualitative and quantitative characterisation for explosion severity and gaseous-solid residues during methane-coal particle hybrid explosions: an approach to estimating the safety degree for underground coal mines," *Process Safety and Environment Protection*, vol. 141, pp. 150–166, 2020.

[3] J. J. Zhang, K. L. Xu, G. Reniers, and G. You, "Statistical analysis the characteristics of extraordinarily severe coal mine accidents (ESCMAs) in China from 1950 to 2018," *Process Safety and Environment Protection*, vol. 133, pp. 332–340, 2020.

[4] S. K. Ray, A. M. Khan, N. K. Mohalik, D. Mishra, S. Mandal, and J. K. Pandey, "Review of preventive and constructive measures for coal mine explosions: an Indian perspective," *International Journal of Mining Science and Technology*, vol. 32, no. 3, pp. 471–485, 2022.

[5] Y. F. Zhu, D. M. Wang, Z. L. Shao et al., "A statistical analysis of coalmine fires and explosions in China," *Process Safety and Environment Protection*, vol. 121, pp. 357–366, 2019.

[6] D. J. Blackley, C. N. Halldin, and A. S. Laney, "Continued increase in prevalence of coal workers' pneumoconiosis in the United States, 1970–2017," *American Journal of Public Health*, vol. 108, no. 9, pp. 1220–1222, 2018.

[7] B. C. Doney, D. Blackley, J. M. Hale et al., "Respirable coal mine dust at surface mines, United States, 1982–2017," *American Journal of Industrial Medicine*, vol. 63, no. 3, pp. 232–239, 2020.

[8] N. B. Hall, D. J. Blackley, C. N. Halldin, and A. S. Laney, "Current review of pneumoconiosis among US coal miners," *Current Environmental Health Reports*, vol. 6, no. 3, pp. 137–147, 2019.

[9] L. Dwyer-Lindgren, A. Bertozzi-Villa, R. W. Stubbs et al., "Trends and patterns of differences in chronic respiratory disease mortality among US counties, 1980-2014," *Journal of the American Medical Association*, vol. 318, no. 12, pp. 1136–1149, 2017.

[10] Y. Shekarian, E. Rahimi, M. Rezaee, W.-C. Su, and P. Roghanchi, "Respirable coal mine dust: a review of respiratory deposition, regulations, and characterization," *Minerals*, vol. 11, no. 7, pp. 696–696, 2021.

[11] Y. Shekarian, E. Rahimi, N. Shekarian, M. Rezaee, and P. Roghanchi, "An analysis of contributing mining factors in coal workers' pneumoconiosis prevalence in the United States coal mines, 1986–2018," *International Journal of Coal Science & Technology*, vol. 8, no. 6, pp. 1227–1237, 2021.

[12] J. Jiang, P. Wang, Y. Pei, R. Liu, L. Liu, and Y. He, "Preparation and performance analysis of a coking coal dust suppressant spray," *International Journal of Coal Science & Technology*, vol. 8, no. 5, pp. 1003–1014, 2021.

[13] G. Zhou, J. F. Ding, Y. L. Ma, S. L. Li, and M. G. Zhang, "Synthesis and performance characterization of a novel wetting cementing agent for dust control during conveyor transport in coal mines," *Powder Technology*, vol. 360, pp. 165–176, 2020.

[14] Q. Bao, W. Nie, C. Q. Liu et al., "The preparation of a novel hydrogel based on crosslinked polymers for suppressing coal dusts," *Journal of Cleaner Production*, vol. 249, article 119343, 2020.

[15] P. F. Wang, Y. D. Jiang, R. H. Liu, L. M. Liu, and Y. C. He, "Experimental study on the improvement of wetting performance of OP-10 solution by inorganic salt additives," *Atmospheric Pollution Research*, vol. 11, no. 6, pp. 153–161, 2020.

[16] Q. Zhou and B. T. Qin, "Coal dust suppression based on water mediums: a review of technologies and influencing factors," *Fuel*, vol. 302, article 121196, 2021.

[17] J. Y. Li and K. Q. Li, "Influence factors of coal surface wettability," *Journal of China Coal Society*, vol. 41, pp. 448–453, 2016.

[18] H. Y. Erbil, "The debate on the dependence of apparent contact angles on drop contact area or three-phase contact line: a review," *Surface Science Reports*, vol. 69, no. 4, pp. 325–365, 2014.

[19] W. M. Cheng, J. Xue, G. Zhou, W. Nie, and J. H. Wen, "Research on the relationship between bituminous coal dust wettability and inorganic mineral content," *Journal of China University of Mining and Technology*, vol. 45, pp. 462–468, 2016.

[20] G. Zhou, H. Qiu, Q. Zhang, M. Xu, J. Y. Wang, and G. Wang, "Experimental investigation of coal dust wettability based on surface contact angle," *Journal of Chemistry*, vol. 2016, Article ID 9452303, 8 pages, 2016.

[21] J. L. Li, F. B. Zhou, and H. Liu, "The selection and application of a compound wetting agent to the coal seam water infusion for dust control," *International Journal of Coal Preparation and Utilization*, vol. 36, no. 4, pp. 192–206, 2016.

[22] Y. R. Chen and W. C. Xia, "An improved sessile drop method for assessing the wettability of heterogeneous coal surface," *Energy Sources, Part A: Recovery, Utilization, and Environmental Effects*, vol. 40, no. 1, pp. 60–67, 2018.

[23] W. M. Cheng, J. Xue, G. Zhou, W. Nie, and L. S. Liu, "Study of coal dust wettability based on FTIR," *Journal of China Coal Society*, vol. 39, no. 11, pp. 2256–2262, 2014.

[24] Z. Gui, R. H. Liu, P. F. Wang, S. X. Gou, W. Shu, and X. H. Tan, "Experimental study on surfactant effect on coal dust wettability," *Journal of Heilongjiang University of Science and Technology*, vol. 26, no. 5, pp. 513–517, 2016.

[25] C. R. Copeland, T. C. Eisele, and S. K. Kawatra, "Suppression of airborne particulates in iron ore processing facilities," *International Journal of Mineral Processing*, vol. 93, no. 3-4, pp. 232–238, 2009.

[26] S. K. Kawatra, *Proceedings of the International Seminar on Mineral Processing Technology and Indo-Korean Workshop on Resource Recycling: Dust in Mineral Processing*, Allied Publishers, Istanbul, 2006.

[27] W. J. Zou, Y. J. Cao, and J. T. Liu, "Surface thermodynamic characterization of fine coal by Washburn dynamic method," *Journal of China Coal Society*, vol. 38, no. 7, pp. 1271–1276, 2013.

[28] J. C. Michel, L. M. Rivière, and M. N. Bellon-Fontaine, "Measurement of the wettability of organic materials in relation to water content by the capillary rise method," *European Journal of Soil Science*, vol. 52, no. 3, pp. 459–467, 2001.

[29] G. J. Zhao, S. S. Bi, J. T. Wu, and X. Li, "A new surface tension measurement system based on capillary rise method," *Journal of Engineering Thermophysics*, vol. 32, no. 4, pp. 546–548, 2011.

[30] C. Wu, X. L. Peng, and G. M. Wu, "Wetting agent investigation for controlling dust of lead-zinc ores," *Transactions of Nonferrous Metals Society of China*, vol. 17, no. 1, pp. 159–167, 2007.

[31] M. Sussman and E. G. Puckett, "A coupled level set and volume-of-fluid method for computing 3D and axisymmetric incompressible two-phase flows," *Journal of Computational Physics*, vol. 162, no. 2, pp. 301–337, 2000.

[32] M. Sussman, "A second order coupled level set and volume-of-fluid method for computing growth and collapse of vapor bubbles," *Journal of Computational Physics*, vol. 187, no. 1, pp. 110–136, 2003.

[33] C. W. Hirt and B. D. Nichols, "Volume of fluid (VOF) method for the dynamics of free boundaries," *Journal of Computational Physics*, vol. 39, no. 1, pp. 201–225, 1981.

[34] L. Chirco, R. Da Vià, and S. Manservisi, "VOF evaluation of the surface tension by using variational representation and Galerkin interpolation projection," *Journal of Computational Physics*, vol. 395, pp. 537–562, 2019.

[35] V. R. Gopala and B. G. M. Wachem, "Volume of fluid methods for immiscible-fluid and free-surface flows," *Chemical Engineering Journal*, vol. 141, no. 1-3, pp. 204–221, 2008.

[36] A. B. Cecala, A. D. O'brien, J. Schall et al., *Dust Control Handbook for Industrial Minerals Mining and Processing*, Department of Health and Human Services, Pittsburgh, 2012.

[37] Y. Yonemoto and T. Kunugi, "Analytical consideration of liquid droplet impingement on solid surfaces," *Scientific Reports*, vol. 7, no. 1, p. 2362, 2017.

[38] J. Chun, J. X. Wang, C. Xu et al., "Theoretical model of maximum spreading diameter on superhydrophilic surfaces," *Acta Physica Sinica*, vol. 70, no. 10, article 106801, 2021.

[39] N. Zheng and H. L. Liu, "Study on rebound behaviour and maximum spreading of shear-thinning fluid droplet impacting on a hydrophobic surface," *Chinese Journal of Theoretical and Applied Mechanics*, vol. 54, no. 7, pp. 1934–1942, 2022.

[40] Y. Q. Li, F. C. Wang, H. Liu, and H. A. Wu, "Nanoparticle-tuned spreading behavior of nanofluid droplets on the solid substrate," *Microfluidics and Nanofluidics*, vol. 18, no. 1, pp. 111–120, 2015.